EES Solar

PAPER

View Article Online
View Journal | View Issue

Cite this: *EES Sol.*, 2025, **1**, 279

Matching electrochemical CO_2 reduction with fluctuating photovoltaic power under natural illumination†

Ya Liu, ‡*[a] Taiping Ye,‡[a] Yifei Liu,‡[b] Xiaohai Zhang,‡[c] Linhong Jiang,[a] Feng Wang,[a] Shengjie Bai[a] and Shaohua Shen[a]

Received 10th January 2025
Accepted 19th March 2025

DOI: 10.1039/d5el00002e

rsc.li/EESSolar

Photovoltaic (PV)-driven electrocatalytic CO_2 reduction enables solar energy storage and green fuel production, but PV fluctuations cause instability, impacting product selectivity and system stability. To tackle this challenge, we propose a novel control strategy that dynamically adjusts the number of operating electrolytic cells. This approach enables real-time matching of PV output with the electrolysis system, stabilizing voltage and current input. The performance of PV modules and electrolyzers was evaluated individually, with results integrated into a simulation model to predict system behavior. Additionally, an outdoor experimental setup was constructed to validate the design under real-world conditions. The system demonstrated the ability to dynamically adjust the number of operating electrolyzers from zero to four in response to fluctuating PV power. Compared to an uncontrolled system with a current density variability of 150 ± 90 mA cm^{-2}, the proposed control strategy stabilized the current density to 210 ± 40 mA cm^{-2}, highlighting its effectiveness in managing fluctuating power inputs.

Broader context

This study introduces a novel strategy for integrating electrochemical CO_2 reduction with fluctuating photovoltaic (PV) power under natural sunlight, addressing key challenges in renewable energy systems. Unlike traditional methods that struggle with unstable power input, poor product selectivity, and operational inefficiencies, our approach dynamically adjusts the number of active electrolyzers based on real-time PV performance. This ensures stable current density and improves product selectivity. For example, our system reduced current density fluctuations from ±90 mA cm^{-2} to ±40 mA cm^{-2}, enhancing overall stability. This practical and scalable solution bridges the gap between solar energy harvesting and sustainable fuel production, offering a transformative step toward efficient solar-driven CO_2 reduction.

1. Introduction

As the urgency of combating climate change grows, there has been a surge of interest in sustainable technologies for carbon dioxide (CO_2) reduction.[1] Among these, photovoltaic (PV)-driven electrochemical CO_2 reduction has emerged as a promising strategy to close the anthropogenic carbon cycle.[2] By harnessing solar energy to power electrochemical processes, this approach enables the conversion of CO_2 into valuable fuels and chemicals, providing an effective pathway for renewable energy storage and utilization.[3] Recent advances in this field have demonstrated the potential of achieving high solar-to-product conversion efficiencies, making it an attractive solution for addressing global energy and environmental challenges. However, due to the complexity of CO_2 reduction products and the intermittent nature of solar energy, the stability, scalability, and cost of such systems are critically influenced by the coupling method between PV systems and electrolyzers.[4–6] This necessitates the exploration of innovative connection strategies to stabilize product selectivity and optimize system performance.

Currently, PV-electrolyzer coupling methods can be broadly categorized into direct coupling and indirect coupling *via* power conversion devices such as DC–DC or DC–AC–DC converters.[7,8] Direct coupling (Fig. 1a) is the simplest configuration, wherein the output of the PV system directly powers the electrolyzer. While this approach minimizes system complexity and cost, it

[a]*International Research Center for Renewable Energy, State Key Laboratory of Multiphase Flow in Power Engineering, Xi'an Jiaotong University, Shaanxi 710049, China. E-mail: yaliu0112@xjtu.edu.cn*

[b]*School of Materials Science and Engineering, Shanghai Jiao Tong University, China*

[c]*PetroChina Shenzhen New Energy Research Institute, Shenzhen, Guangdong 518000, China*

† Electronic supplementary information (ESI) available: Details of catalytic performance evaluation indexes, system mathematical models, modelling methods, test methods, test instruments, ESI data and graphs. See DOI: https://doi.org/10.1039/d5el00002e

‡ These authors contributed equally: Ya Liu, Taiping Ye, Yifei Liu, Xiaohai Zhang.

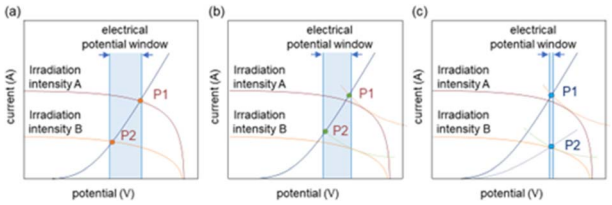

Fig. 1 Schematic diagram of system *I*–*V* characteristics for different connection methods (a) direct coupling (b) indirect coupling (c) this working design method (d) comparison of selective performance of electrolytic cell for carbon monoxide under different control modes.

suffers from significant drawbacks, including large voltage fluctuations under variable solar irradiance.[3,8,9] These fluctuations adversely impact system stability, reduce solar energy utilization efficiency, and lead to poor product selectivity in CO_2 electroreduction.[10–13] Indirect coupling (Fig. 1b) addresses some of these issues by incorporating power management systems, which improve flexibility and enhance voltage matching efficiency.[14] This configuration also increases the system's power output to some extent.

However, indirect coupling introduces additional energy losses and costs, and it fails to fully resolve the issue of drastic changes in product selectivity caused by voltage input variations.[15–17] These challenges underline the limitations of existing coupling strategies in balancing efficiency, cost, stability, and selectivity, highlighting the need for more advanced solutions.[5,18,19] To address these challenges, we propose a novel PV-electrolyzer coupling method (Fig. 1c) that employs a specially designed coupling control module. This module dynamically adjusts the number of electrolyzer units connected to the PV system in response to fluctuating solar irradiance, thereby stabilizing the input voltage to the electrolyzers. By maintaining a consistent operating voltage, the approach effectively improves product selectivity and enhances system stability under natural light conditions.

2. System design and performance

2.1. Catalyst synthesis and electrode preparation

Fig. 2 shows the main steps in the preparation of the anode. Detailed synthesis procedures are given in Methods. The $Ni_3Fe(OH)_9$ electrode exhibits extremely high catalytic activity and a very low overpotential for the OER in an alkaline electrolyte. Only an overpotential of 200 mV (relative to SHE.) is required for the reaction to occur. Therefore, a $Ni_3Fe(OH)_9$ anode was prepared using nickel foam with a thickness of 1.6 mm and a bulk density of 0.45 g cm^{-3} (Fig. 2).[20,21] The treated anode exhibits a three-dimensional (3D) structure, which provides a large specific surface area and abundant active sites, facilitating electrolyte penetration and gas diffusion, thereby enhancing the overall catalytic efficiency of the system. Studies have shown that this anode demonstrates exceptional stability under high current densities, maintaining high catalytic activity even after prolonged electrolysis. Notably, $Ni_3Fe(OH)_9$ remains stable and operational at current densities as high as 500 mA cm^{-2}.

The cathode electrode uses a GDE structure, and the preparation process is divided into substrate hydrophobic pretreatment, catalyst synthesis and cathode material preparation. The carbon paper substrate was hydrophobically pretreated to a certain extent in order to prevent overflow and prolong the lifetime of the cathode.[22,23] Fig. S4† shows the phenomenon when flooding occurs at the cathode side. The state of carbon paper at different stages of electrode pre-treated is shown in Fig. S5.† Cu–KOH catalyst, which has good selectivity towards ethylene and a certain stability, was chosen as the cathode catalyst. To demonstrate that this system is also applicable to other catalytic processes, a Ag catalyst was prepared using silver powder.

2.2. Photovoltaic-driven electrocatalytic carbon dioxide reduction stack system

Reduction electrolysis cell system is shown in Fig. 3a, where the photovoltaic module is directly-driven to the electrolysis cell assembly through a control module. That the operating point of the device remains near the Maximum Power Point (MPP). This approach optimizes system performance and stabilizes the ethylene selectivity of the electrolysis cells. Fig. 3b presents the system device diagram, illustrating the connections between components designed to meet testing requirements under various conditions.

The electrolysis cell assembly consists of multiple individual electrolysis cells. In the system, the reactants – such as CO_2 as, electrolyte flow, and the resulting products (both gaseous and liquid) – are connected in series between individual electrolysis cells.[24] The power input to the electrolysis cell module, supplied by the control module, is connected in parallel. This parallel configuration facilitates control of the number of electrolysis cells involved in the reaction, while the series configuration improves reactant feed and product collection.[25,26]

Compared to photovoltaic-driven water electrolysis for hydrogen production, the direct coupling of PV with CO_2 reduction cells presents a more complex product range, with product selectivity highly sensitive to factors such as current, voltage, catalysts, and electrolytes.[27–30] To mitigate the effect of current on product selectivity, the current density applied to the electrolysis cell assembly is carefully controlled. Based on the design concept, an outdoor experimental setup was

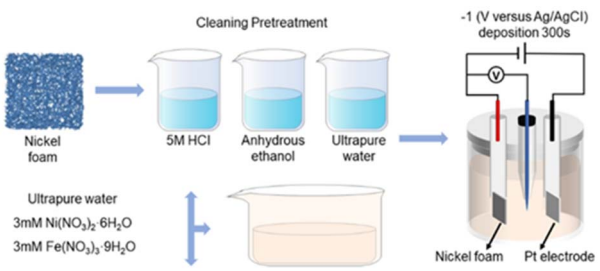

Fig. 2 $Ni_3Fe(OH)_9$ anode preparation steps.

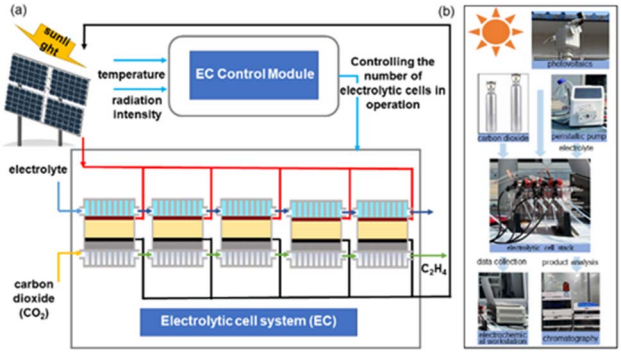

Fig. 3 (a) Schematic diagram of a photovoltaic-driven electrocatalytic carbon dioxide reduction electrolysis cell system; (b) physical diagram of the carbon dioxide reduction stack and test platform.

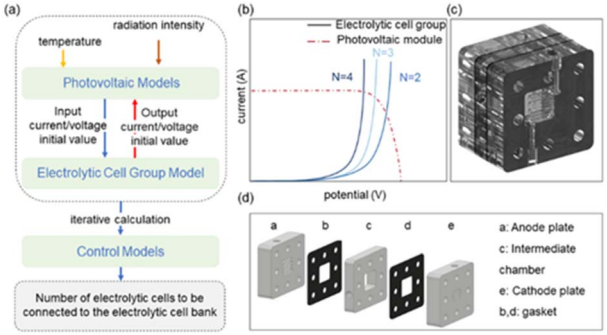

Fig. 4 Control system and electrolysis cell. (a) Functional diagram of the coupled control model. (b) Schematic diagram of power point variation of the system with different number of electrolytic cells accessed. (c) A self-designed acrylic flow electrolyzer. (d) Self-designed plexiglass flow electrolytic cell.

constructed.[4] The experiment used photovoltaic cells for real-time power supply, enhanced by an outdoor tracking system to maximize sunlight utilization and achieve optimal output power. The photovoltaic cells were connected in parallel with the electrolysis cell array, with a microcontroller managing the relay to control the connection of varying numbers of electrolysis cells.

For testing and data collection, a commercial photonic solar radiation sensor measured the irradiance intensity, while a Pt100 adhesive temperature sensor monitored the operating temperature of the photovoltaic modules. The electrical circuit was linked to a Swiss Metrohm AUTOLAB electrochemical workstation, which continuously recorded current data over time, facilitating subsequent calculations of faradaic efficiency (FE). The microcontroller was designed to output results every 5 seconds based on pre-set parameters, including temperature, irradiance intensity, and the number of electrolysis cells connected, couple with remote control software, this setup enabled real-time remote monitoring. The equipment and components used in the system are shown in Fig. S1, S2, S7, S8 and S10.† The performance of a photovoltaic-driven electrochemical system is primarily influenced by its operating point during actual operation. By integrating the photovoltaic model with the electrolytic cell group model, the system's operating point can be determined using the IV estimation algorithm. This operating point corresponds to the intersection of the IV curves of the photovoltaic module and the electrolytic cell. For optimal efficiency, the photovoltaic device should operate near the maximum power point, where energy conversion efficiency is maximized.[4]

The operating point data shown in Fig. 4a, a must be obtained using a coupled photovoltaic model and an electrolysis cell array model. The operating point data is processed and the control boundary conditions are set. The results are calculated iteratively and the control results are output *via* the control module. The number of electrolytic cells, effectively optimizing the operating point under direct coupling of the photovoltaic and electrolytic cell groups (Fig. 4b), while also stabilizing the input current to the electrolytic cells.[31]

During the electrocatalytic CO_2 reduction process, the electrolytic cell module may experience overflow due to mass transfer limitations, catalyst degradation, or sudden fluctuations in input current. Such issues can disrupt the production of target products and lead to material loss. To enhance mass transfer within the electrolytic cell, structural and material modifications have been implemented in the reactor design, as illustrated in Fig. 4c.

In contrast to the original flow electrolyzer's cathode plate design, where the cathode chamber has been changed from the original serpentine pipeline layout to a cubic cavity structure, increasing the contact area between the gas and the catalyst, thereby extending the catalyst's lifespan (Fig. 4d). This design was chosen because, for a reaction area of only 1 cm^2, the cavity structure is more straightforward to design and manufacture while achieving mass transfer efficiencies comparable to those of flow channel structures. Experimental results revealed that, in electrochemical tests with small reaction areas, flow channels may have sections that are not in direct contact with the gas, preventing the reaction from occurring at those points. This phenomenon leads to electrode overflow, as illustrated in ESI Fig. S5.† Original serpentine pipeline structures, compared to cubic cavity designs, are more susceptible to electrode overflow, particularly in systems with the same reaction area.

The electrolysis cell assembly is constructed from transparent acrylic, allowing clear observation of the reaction process and facilitating the detection of electrode. Overflow or the need for electrode replacement.

2.3. Performance of the electrocatalytic carbon dioxide reduction electrolyser

Current and voltage parameters are crucial control factors for adjusting the number of electrolytic cells integrated into the system. The selection of initial current density and voltage boundary conditions for the coupled control model should be based on experimental results from the electrolytic cell, ensuring that the simulation experiments align with the target of maintaining stable ethylene selectivity. To identify the optimal operating parameters for ethylene production, multiple performance tests were conducted on the Cu–KOH gas diffusion electrode (GDE) cathode under constant current density and

constant pressure conditions. A 1 M potassium hydroxide (KOH) solution was used as the electrolyte, and the experimental results are shown in Fig. 5a and b. Detailed data supporting the reproducibility of these results is provided in the ESI.† For industrial applications, a current density greater than 200 mA cm^{-2} is typically required to make the process economically viable. Consequently, the constant current density tests began with an initial value of 200 mA cm^{-2}, incrementing by 25 mA cm^{-2} steps until reaching 300 mA cm^{-2}. As the current density increased, the Faraday efficiency (FE) of ethylene production initially increased and then decreased. A peak Faraday efficiency was observed at a current density of 250 mA cm^{-2}, where ethylene production was most efficient.

Since the electrolytic cell stack consists of multiple parallel-connected cells, a constant voltage test was also conducted to evaluate the corresponding changes in current density and Faraday efficiency under varying voltage conditions. The constant voltage range was set between 3.3 V and 3.7 V, with a step size of 0.1 V, while keeping other experimental conditions consistent with those used in the constant current test. The results, shown in Fig. 5b, revealed that the single electrolytic cell performed optimally between 3.5 V and 3.6 V, with a current density of approximately 250–260 mA cm^{-2} at this voltage range. There is a linear relationship between current density and voltage. This confirms that current density is a critical parameter for stabilizing ethylene selectivity and aligns with the initial *I–V* curve model of the electrolyzer, validating the electrolyzer's design. Stability tests were carried out on single cells and cell stacks under optimal operating conditions, as shown in Fig. 5c and d. This shows that stabilizing the voltage and current of the cell stack can greatly improve the selectivity and stability of the cell.

3. System model construction

The system model is composed of three main components: the photovoltaic (PV) model, the electrolytic cell group model, and the control module model. Once the initial design of the model is completed, its accuracy needs to be validated using experimental data, and the model is subsequently optimized based on the results.

For model verification, a sunny day was selected for testing, during which the photovoltaic module was scanned in reverse using linear sweep voltammetry (LSV) to obtain the photovoltaic *I–V* curve. Real-time irradiance intensity and temperature were measured using an independent solar radiation sensor and a Pt100 adhesive temperature sensor. The measurement results for a particular day are presented in Fig. 6a. Based on these test results, the performance parameters of the commercial PV panel under Standard Test Conditions (STC) were compared with those of the PV model calculated according to the EN50530 standard. The parameters used for the PV model in this study are summarized in Table S1.† For detailed calculation methods, please refer to the ESI.[3,14,31]† These parameters were then applied to construct the photovoltaic model under the ISDM (Integrated System Dynamic Model), and the output results are shown in Fig. 6b.

For the electrolytic cell model, cyclic voltammetry (CV) was employed to collect data for individual electrolytic cells and electrolytic cell groups with varying numbers of connected cells. Each test involved scanning from the open-circuit voltage (V_{ocp}) to a cell voltage of 4.5 V at a scan rate of 0.05 V s^{-1}.

The CV curves for electrolytic cells with different numbers of cells were obtained after four scans, starting from the open-circuit voltage and progressing to the specified potential. The data points under voltage conditions ranging from 0 to 4 V, which matched the actual test results, were selected to generate multiple *I–V* curves for electrolytic cells with varying configurations (Fig. 6c).

A polynomial curve was fitted to the *I–V* curves of the electrolytic cell system using the least squares method. The model parameters were adjusted to achieve the best fit, and the following formula was derived for the *I–V* curve of the electrolyzer bank within the reaction system:

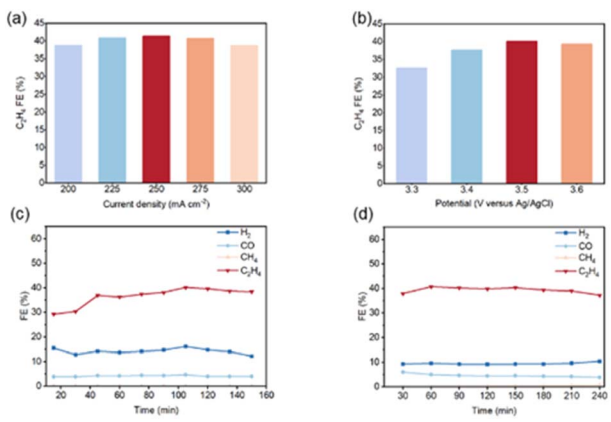

Fig. 5 Catalytic performance of electrolytic cell set. (a) Single cell constant current test. (b) Single electrolyzer constant voltage test. (c) Stability test under constant voltage (3.6 V) of single electrolytic cell. (d) Stability test under constant voltage (3.6 V) of electrolytic cell set.

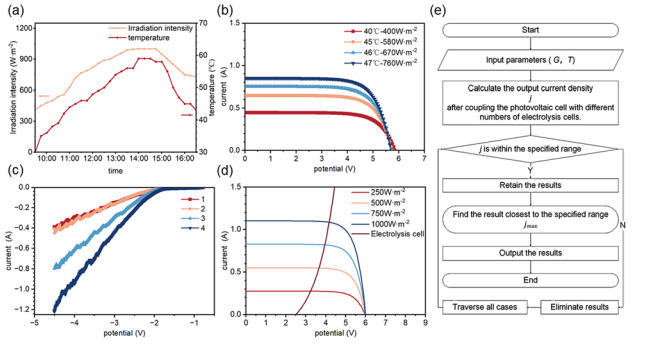

Fig. 6 Simulation model construction. (a) Variation of daily irradiation intensity and PV operating temperature. (b) ISDM PV *I–V* characteristic curve. (c) *I–V* characteristic curve of electrolytic cell set with different number of electrolytic cells connected to it. (d) Variation of working point of electrolytic cell set under different specifications of PV module working conditions. (e) Schematic diagram of the operation logic of the coupled control model.

$$I_{\text{Cu-KOH}} = \begin{cases} 0 & V \le 2.02 \\ (0.12280N_{\text{p}} + 0.04420)\left(\dfrac{V}{N_{\text{s}}} - 2.02\right) & V > 2.02 \end{cases} \quad (1)$$

where: I is the current of the electrolytic cell bank; V is the voltage of the electrolytic cell bank; N_{s} is the number of series electrolytic cells in the electrolytic cell bank; N_{p} is the number of parallel electrolytic cells in the electrolytic cell bank.[17]

The formula and related data were then substituted into a prepared program to simulate the electrolyzer bank of the reaction system.

The simulation software was developed in C language, as outlined in Fig. 6e. In this model, current density was used as the key control parameter.

The control system continuously receives real-time irradiance and temperature data from the photovoltaic module and calculates the output current density of the photovoltaic cells, which are coupled with different numbers of electrolytic cells. Based on a predefined range of current values, the system determines the optimal number of electrolytic cells to be connected. This approach enables the system to dynamically adjust the number of electrolytic cells. To enhance the efficiency of the iterative process, the Newton method was employed to improve the speed of convergence. The expression for this method is as follows:

$$x_{n+1} = x_n - \frac{f(x_n)}{f'(x_n)} \quad (2)$$

where x_n is the value at the nth iteration, $f(x_n)$ is the iteration calculation formula, and $f'(x_n)$ is the $f(x_n)$ derivative.

Fig. 6d shows the working condition diagram of the system coupling realized by regulating the parameters of PV panels without changing the number of electrolytic cell groups, and it can be clearly seen that, the electrolytic cell groups change with the parameters of the and PV modules, and the voltage and current input into the electrolytic cell groups change drastically. Compared with the coupling strategy proposed in this study (Fig. 4b), the above method is not conducive to stabilizing the selectivity of the electrolytic cell products, and at the same time, it will greatly reduce the service life of the catalyst.

3.1. System simulation test

An outdoor experiment was conducted for 2.5 hours on a specific day in April 2024, from 15:00 to 17:30, during which solar irradiance and temperature were continuously monitored. An outdoor control test platform was established for this experiment. The performance data from the tested PV panels was input into the simulation testing software, with the control program set to operate within a current density range of 180 mA cm^{-2} to 250 mA cm^{-2}.

As solar irradiance fluctuated, the control module adjusted the input current to the electrolysis cells accordingly. When the solar irradiance was high, the number of electrolysis cells connected reached its maximum, and the current density could not be maintained below 250 mA cm^{-2}. In cases where there was a risk of overflow in the electrolysis cell assembly, the control module disconnected the electrolysis cells from the photovoltaic module, bringing the input current density to zero to protect the assembly (Fig. 7a). When the current density was within an adjustable range, the number of electrolysis cells connected to the system changed in sync with the solar irradiance, decreasing from four to zero (Fig. 7b), achieving real-time synchronous control of the input current density to the electrolysis cell assembly.

Based on the relationship between the solar irradiance of the PV panels under controlled conditions (varying numbers of electrolysis cells) and uncontrolled conditions (four electrolysis cells connected simultaneously), we calculated the current density of the electrolysis cell assembly for both scenarios (Fig. 7c). Compared to the simulation results under uncontrolled conditions, the controlled system exhibited excellent current control in regions of relatively low irradiance, maintaining the current within the specified range. The control system theoretically achieves effective regulation of the current density in the photovoltaic-coupled electrochemical system.

Since only a single system was designed, simultaneous experiments under both controlled and uncontrolled conditions were not feasible. Therefore, performance data for the PV panels was recorded during a unified time period. Using an ITECH IT6512C programmable DC power supply and the accompanying SAS 1000 simulation software, we simulated the power supply from the outdoor PV panels during the outdoor experiment on April 2024 from 15:00 to 17:30.

Performance testing was conducted under uncontrolled conditions, with results presented in Fig. 7d. Compared to the uncontrolled system, the results obtained under controlled conditions were slightly higher. However, when abrupt changes in irradiance led to sudden shifts in current, the controlled system maintained stability, while the uncontrolled system exhibited significant declines, with an irreversible decrease in ethylene selectivity. The controlled system not only stabilized ethylene selectivity but also enhanced the stability of the electrolysis cell assembly and the longevity of the electrodes.

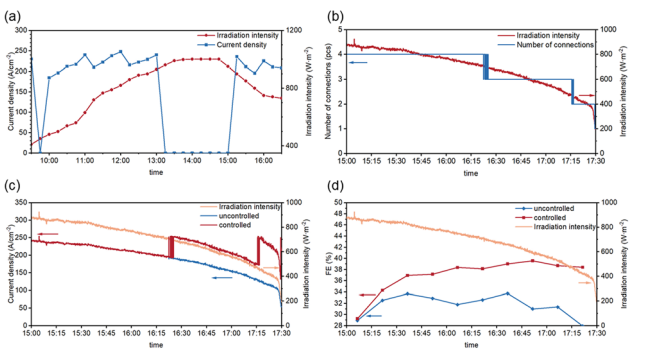

Fig. 7 Simulation test results. (a) Variation of current density with controlled conditions. (b) Variation of the number of electrolytic cells connected under controlled conditions. (c) Variation of current density with and without control condition. (d) Comparison of ethylene selectivity with and without control condition.

To validate the design of this study and assess the system's applicability to different catalytic materials, we synthesized an Ag-based catalyst following the methods reported in the literature and integrated it into the electrolyzer system.[31–33] Under identical experimental conditions, its electrocatalytic performance was evaluated to determine the system's compatibility with commercial catalysts.

Furthermore, to investigate the system's performance under varying weather conditions, we measured and recorded the local solar irradiance and ambient temperature throughout February 28 under cloudy conditions. Using an Anitech IT6512C programmable DC power supply and SAS 1000 simulation software, the recorded data were input to simulate the power output of an outdoor photovoltaic (PV) panel on that day. Under the same power supply conditions, different connection configurations between the electrolyzer and power source were tested, including direct connection, indirect connection, and the control strategy proposed in this study. Ag-based catalysts were used to evaluate CO selectivity under these different configurations while keeping all other experimental conditions constant.

As shown in Fig. 8a, electrochemical CO_2 reduction proceeded as long as the PV module provided power, even under cloudy conditions. However, in both direct and indirect connection modes, rapid fluctuations in irradiance led to a significant and irreversible decline in catalyst selectivity. In contrast, the proposed control strategy effectively stabilized catalyst selectivity to some extent. To further investigate catalyst performance, we conducted repeated experiments on catalysts that had undergone prior regulation by the control system (Fig. 8b). While a slight decrease in selectivity was observed, the control module successfully maintained relative stability, demonstrating the effectiveness of the proposed strategy in mitigating the impact of irradiance fluctuations.

4. Methods

4.1. Anode synthesis

Nickel foam was initially cleaned using a 5 M hydrochloric acid solution (AR, Shanghai Hushi) and anhydrous ethanol (AR, Tianjin Tianli) with ultrasonic treatment for over 5 minutes. After cleaning, the nickel foam was rinsed with deionized water and dried to remove any surface residues. Next, a mixed aqueous solution of 3 mM nickel(II) nitrate hexahydrate ($Ni(NO_3)_2 \cdot 6H_2O$, AR, Shanghai Hushi) and 3 mM iron(III) nitrate nonahydrate ($Fe(NO_3)_3 \cdot 9H_2O$, 99.99%, Shanghai Aladdin) was prepared. The cleaned nickel foam was used as the cathode, while a platinum sheet served as the anode. The prepared mixed aqueous solution acted as the electrolyte, and the electrodeposition was conducted under constant temperature and potential conditions at 10 °C and −1 V (relative to Ag/AgCl reference electrode) for 300 seconds. After electro-deposition, the electrode materials were rinsed with deionized water, dried with nitrogen gas (N_2), and left to air dry, resulting in an anode suitable for experimentation.

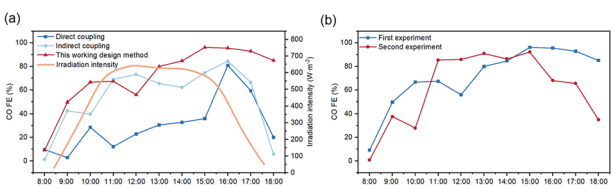

Fig. 8 (a) Comparison of selective performance of electrolytic cell for carbon monoxide under different control modes; (b) repeated experiments with used catalysts under the same experimental conditions under the control method of this work.

4.2. Cathode catalyst

A solution was prepared following the ratio of 60 mg Cu, 60 mg KOH, 60 mg Nafion, and 2 mL isopropanol. This catalyst solution was then spray-coated onto carbon paper at a loading density of 1 mg cm^{-2} using a spray gun under constant temperature conditions at 70 °C. The coated carbon paper was allowed to air dry overnight before proceeding with subsequent experiments.

5. Conclusions

This study presents a novel control strategy that directly couples photovoltaic (PV) modules with electrochemical CO_2 reduction systems, achieving stable ethylene synthesis under specific environmental conditions by adjusting the number of electrolysis cells connected to the PV-coupled electrochemical system. We established a model for the PV-coupled electrochemical CO_2 reduction system, comprising PV panels and varying numbers of electrolysis cells. Corresponding coupling control software was designed to enable efficient management of the PV-coupled electrochemical CO_2 reduction system. The design of the simulation and testing model plays a crucial role in system optimization, allowing for the validation of the theoretical feasibility of the proposed control model using actual test data for simulation experiments. Practical reaction apparatus was constructed for outdoor testing in natural environmental conditions. The selectivity for the gas-phase product C_2H_4 was consistently maintained between 35% and 40%. Compared to an uncontrolled system with a current density variability of 150 ± 90 mA cm^{-2}, the proposed control strategy stabilized the current density to 210 ± 40 mA cm^{-2}, highlighting its effectiveness in managing fluctuating power inputs. Compared to systems without a control mechanism, the controlled reaction system exhibited higher selectivity for C_2H_4, particularly maintaining stability during periods of lower irradiance. This system demonstrates the ability to stably synthesize specific hydrocarbon products under variable conditions, providing valuable insights for the industrial application of photovoltaic direct coupling in electrochemical CO_2 reduction technologies. Future research may focus on further enhancing the efficiency and selectivity of the system, exploring alternative catalysts, and scaling up the technology for broader industrial applications.

Data availability

The data supporting this article is included as part of the ESI.†

Author contributions

The manuscript was written through contributions of all authors. All authors have given approval to the final version of the manuscript.

Conflicts of interest

There are no conflicts to declare.

Acknowledgements

This work is supported by the National Key R&D Program of China (2024YFF0506100), the Sichuan Science and Technology Program (No. 2024YFHZ0037), the Natural Science Basic Research Program of Shaanxi (No. 2024JC-YBMS-284), the Key Research and Development Program of Shaanxi (No. 2024GH-YBXM-02), and the Fundamental Research Funds for the Central Universities.

References

1 Z. Xu, R. Lu, Z. Y. Lin, W. Wu, H. J. Tsai, Q. Lu, Y. C. Li, S. F. Hung, C. Song, J. C. Yu, Z. Wang and Y. Wang, Electroreduction of CO_2 to methane with triazole molecular catalysts, *Nat. Energy*, 2024, **9**(11), 1397–1406.

2 J. Guerrero, E. Bajard, N. Schneider, F. Dumoulin, D. Lincot, U. Isci, M. Robert and N. Naghavi, Multifunctional Photovoltaic Window Layers for Solar-Driven Catalytic Conversion of CO_2: The Case of CIGS Solar Cells, *ACS Energy Lett.*, 2023, **8**(8), 3488–3493.

3 J. Kim, S. Jeong, M. Beak, J. Park and K. Kwon, Performance of photovoltaic-driven electrochemical cell systems for CO_2 reduction, *Chem. Eng. J.*, 2022, **428**, 130259.

4 I. Holmes-Gentle, S. Tembhurne, C. Suter and S. Haussener, Kilowatt-scale solar hydrogen production system using a concentrated integrated photoelectrochemical device, *Nat. Energy*, 2023, **8**(6), 586–596.

5 G. M. Sriramagiri, W. Luc, F. Jiao, K. Ayers, K. D. Dobson and S. S. Hegedus, Computation and assessment of solar electrolyzer field performance: comparing coupling strategies, *Sustainable Energy Fuels*, 2019, **3**(2), 422–430.

6 A. C. Lourenço, A. S. Reis-Machado, E. Fortunato, R. Martins and M. J. Mendes, Sunlight-driven CO_2-to-fuel conversion: Exploring thermal and electrical coupling between photovoltaic and electrochemical systems for optimum solar-methane production, *Mater. Today Energy*, 2020, **17**, 100425.

7 R. García-Valverde, C. Miguel, R. Martínez-Béjar and A. Urbina, Optimized photovoltaic generator–water electrolyser coupling through a controlled DC–DC converter, *Int. J. Hydrogen Energy*, 2008, **33**(20), 5352–5362.

8 L. Arriaga, W. Martinez, U. Cano and H. Blud, Direct coupling of a solar-hydrogen system in Mexico, *Int. J. Hydrogen Energy*, 2007, **32**(13), 2247–2252.

9 X. Yan, L. Tian, F. Xue, J. Huang, R. Zhao, X. Guan, J. Shi, W. Chen and M. Liu, *In situ* hydrogen production in all-level-humidity air: integrating atmospheric water harvesting with photocatalysis, *EES Catal.*, 2025, **10**, 1039.

10 C. Xie, Z. Niu, D. Kim, M. Li and P. Yang, Surface and Interface Control in Nanoparticle Catalysis, *Chem. Rev.*, 2020, **120**(2), 1184–1249.

11 M. Ma and B. Seger, Rational Design of Local Reaction Environment for Electrocatalytic Conversion of CO_2 into Multicarbon Products, *Angew. Chem., Int. Ed.*, 2024, e202401185.

12 W. Fang, W. Guo, R. Lu, Y. Yan, X. Liu, D. Wu, F. M. Li, Y. Zhou, C. He, C. Xia, H. Niu, S. Wang, Y. Liu, Y. Mao, C. Zhang, B. You, Y. Pang, L. Duan, X. Yang, F. Song, T. Zhai, G. Wang, X. Guo, B. Tan, T. Yao, Z. Wang and B. Y. Xia, Durable CO_2 conversion in the proton-exchange membrane system, *Nature*, 2024, **626**(7997), 86–91.

13 M. Sun, J. Cheng and M. Yamauchi, Gas diffusion enhanced electrode with ultrathin superhydrophobic macropore structure for acidic CO_2 electroreduction, *Nat. Commun.*, 2024, **15**(1), 491.

14 A. Mohammadi and M. Mehrpooya, A comprehensive review on coupling different types of electrolyzer to renewable energy sources, *Energy*, 2018, **158**, 632–655.

15 A. R. Jordehi, Parameter estimation of solar photovoltaic (PV) cells: A review, *Renewable Sustainable Energy Rev.*, 2016, **61**, 354–371.

16 K. Ishaque and Z. Salam, An improved modeling method to determine the model parameters of photovoltaic (PV) modules using differential evolution (DE), *Sol. Energy*, 2011, **85**(9), 2349–2359.

17 O. Atlam and M. Kolhe, Equivalent electrical model for a proton exchange membrane (PEM) electrolyser, *Energy Convers. Manage.*, 2011, **52**(8–9), 2952–2957.

18 B. Kim, H. Seong, J. T. Song, K. Kwak, H. Song, Y. C. Tan, G. Park, D. Lee and J. Oh, Over a 15.9% Solar-to-CO Conversion from Dilute CO_2 Streams Catalyzed by Gold Nanoclusters Exhibiting a High CO_2 Binding Affinity, *ACS Energy Lett.*, 2019, **5**(3), 749–757.

19 W. H. Cheng, M. H. Richter, I. Sullivan, D. M. Larson, C. Xiang, B. S. Brunschwig and H. A. Atwater, CO_2 Reduction to CO with 19% Efficiency in a Solar-Driven Gas Diffusion Electrode Flow Cell under Outdoor Solar Illumination, *ACS Energy Lett.*, 2020, **5**(2), 470–476.

20 Q. He, H. Li, Z. Hu, L. Lei, D. Wang and T. Li, Highly Selective CO_2 Electroreduction to C_2H_4 Using a Dual-Sites Cu(II) Porphyrin Framework Coupled with Cu_2O Nanoparticles *via* a Synergetic-Tandem Strategy, *Angew. Chem., Int. Ed.*, 2024, **63**(33), e202407090.

21 C. Zhan, F. Dattila, C. Rettenmaier, A. Herzog, M. Herran, T. Wagner, F. Scholten, A. Bergmann, N. López and C. B. Roldan, Key intermediates and Cu active sites for CO_2 electroreduction to ethylene and ethanol, *Nat. Energy*, 2024, **9**, 1485–1496.

22 P. Papangelakis, R. K. Miao, R. Lu, H. Liu, X. Wang, A. Ozden, S. Liu, N. Sun, C. P. O'Brien, Y. Hu, M. Shakouri, Q. Xiao, M. Li, B. Khatir, J. E. Huang, Y. Wang, Y. C. Xiao, F. Li, A. S. Zeraati, Q. Zhang, P. Liu, K. Golovin, J. Y. Howe, H. Liang, Z. Wang, J. Li, E. H. Sargent and D. Sinton,

Improving the SO_2 tolerance of CO_2 reduction electrocatalysts using a polymer/catalyst/ionomer heterojunction design, *Nat. Energy*, 2024, **9**(8), 1011–1020.

23 Y. Kim, E. W. Lees, C. Donde, A. M. L. Jewlal, C. E. B. Waizenegger, B. M. W. De Hepcée, G. L. Simpson, A. Valji and C. P. Berlinguette, Integrated CO_2 capture and conversion to form syngas, *Joule*, 2024, **8**(11), 3106–3125.

24 Y. Song, S. Fang, N. Xu, M. Wang, S. Chen, J. Chen, B. Mi and J. Zhu, Solar transpiration–powered lithium extraction and storage, *Science*, 2024, **385**(6716), 1444–1449.

25 M. Schreier, F. Héroguel, L. Steier, S. Ahmad, J. S. Luterbacher, M. T. Mayer, J. Luo and M. Grätzel, Solar conversion of CO_2 to CO using Earth-abundant electrocatalysts prepared by atomic layer modification of CuO, *Nat. Energy*, 2017, **2**(7), 17087.

26 B. Liu, L. Ma, H. Feng, Y. Zhang, J. Duan, Y. Wang, D. Liu and Q. Li, Photovoltaic-Powered Electrochemical CO_2 Reduction: Benchmarking against the Theoretical Limit, *ACS Energy Lett.*, 2023, **8**(2), 981–987.

27 C. P. O'Brien, R. K. Miao, A. Shayesteh Zeraati, G. Lee, E. H. Sargent and D. Sinton, CO_2 Electrolyzers, *Chem. Rev.*, 2024, **124**(7), 3648–3693.

28 W. Liu, Z. Lv, C. Wang, C. Sun, C. Tian, X. Wang, H. Yu, X. Feng, W. Yang and B. Wang, Industrial-Level Modulation of Catalyst-Electrolyte Microenvironment for Electrocatalytic CO_2 Reduction: Challenges and Advancements, *Adv. Energy Mater.*, 2024, **14**(44), 2402942.

29 T. Yan, X. Chen, L. Kumari, J. Lin, M. Li, Q. Fan, H. Chi, T. J. Meyer, S. Zhang and X. Ma, Multiscale CO_2 Electrocatalysis to C_{2+} Products: Reaction Mechanisms, Catalyst Design, and Device Fabrication, *Chem. Rev.*, 2023, **123**(17), 10530–10583.

30 S. You, J. Xiao, S. Liang, W. Xie, T. Zhang, M. Li, Z. Zhong, Q. Wang and H. He, Doping engineering of Cu-based catalysts for electrocatalytic CO_2 reduction to multi-carbon products, *Energy Environ. Sci.*, 2024, **17**(16), 5795–5818.

31 T. Maeda, H. Ito, Y. Hasegawa, Z. Zhou and M. Ishida, Study on control method of the stand-alone direct-coupling photovoltaic – Water electrolyzer, *Int. J. Hydrogen Energy*, 2012, **37**(6), 4819–4828.

32 M. Fan, J. E. Huang, R. K. Miao, Y. Mao, P. Ou, F. Li, X. Y. Li, Y. Cao, Z. Zhang, J. Zhang, Y. Yan, A. Ozden, W. Ni, Y. Wang, Y. Zhao, Z. Chen, B. Khatir, C. P. O'Brien, Y. Xu, Y. C. Xiao, G. I. N. Waterhouse, K. Golovin, Z. Wang, E. H. Sargent and D. Sinton, Cationic-group-functionalized electrocatalysts enable stable acidic CO2 electrolysis, *Nat. Catal.*, 2023, **6**(9), 763–772.

33 M. Zhong, K. Tran, Y. Min, C. Wang, Z. Wang, C. T. Dinh, P. De Luna, Z. Yu, A. S. Rasouli, P. Brodersen, S. Sun, O. Voznyy, C. S. Tan, M. Askerka, F. Che, M. Liu, A. Seifitokaldani, Y. Pang, S. C. Lo, A. Ip, Z. Ulissi and E. H. Sargent, Accelerated discovery of CO2 electrocatalysts using active machine learning, *Nature*, 2020, **581**(7807), 178–183.